CANDU WITH SUPERCRITICAL WATER COOLANT: CONCEPTUAL DESIGN FEATURES

by
N. Spinks

AECL
Chalk River Laboratories

Introduction

An advanced CANDU reactor, with supercritical water as coolant, has many attractive design features. The pressure exceeds 22 MPa but coolant temperatures in excess of 370°C can be reached without encountering the two-phase region with its associated fuel-dry-out and flow-instability problems. Increased coolant temperature leads to increased plant thermodynamic efficiency reducing unit energy cost through reduced specific capital cost and reduced fueling cost. Increased coolant temperature leads to reduced void reactivity via reduced coolant in-core density. Light water becomes a coolant option. To preserve neutron economy, an advanced fuel channel is needed and is described below. A supercritical-water-cooled CANDU can evolve as fuel capabilities evolve to withstand increasing coolant temperatures.

CANTHERM Fuel Channel

With a conventional CANDU fuel channel, an increase in coolant pressure and temperature would require an increase in pressure-tube thickness and a loss of neutron economy. To preserve neutron economy, especially at high coolant temperatures, a change in fuel channel design is needed. The CANTHERM insulated fuel channel, shown in figure 1, is currently under development at AECL. It has no calandria tube and the pressure tube, in contact with the cool heavy-water moderator, is insulated from the high-temperature coolant. Such a fuel channel could be employed to increase coolant temperatures and pressures in a conventional CANDU primary heat transport system or it could be employed in a redesign at supercritical coolant conditions.

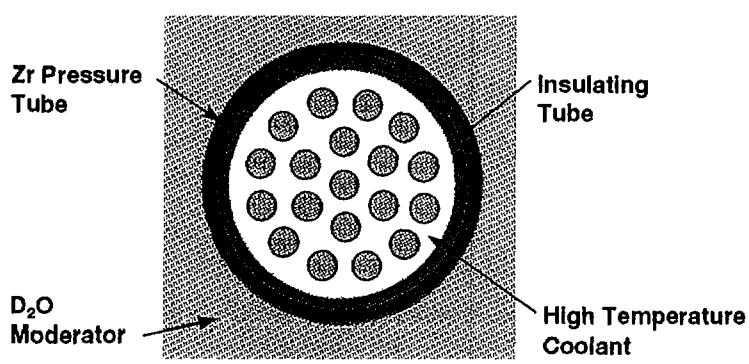

Figure 1: CANTHERM Insulated Fuel Channel

Supercritical CANDU Evolution

Figure 2, based on the properties of light water, illustrates how CANDU could evolve in terms of coolant temperature and enthalpy from conventional pressures and temperatures to supercritical pressures and temperatures. Two stages of development of a supercritical-cooled CANDU have been chosen with coolant core-mean temperatures near 400°C and 500°C. These are dubbed Mark 1 and Mark 2 respectively. They are based on heavy or light water coolant at a nominal pressure of 25 MPa. Mark 1 transfers heat from a heavy water primary system to a light water secondary system at 19 MPa and is expected to operate with conventional or near-conventional zirconium alloy clad fuel. Mark 2 requires advanced fuel and operates with heavy water to light water or light water to light water in an indirect cycle or with light water in a direct cycle. The Mark 1 concept has been developed further and is the subject of this paper.

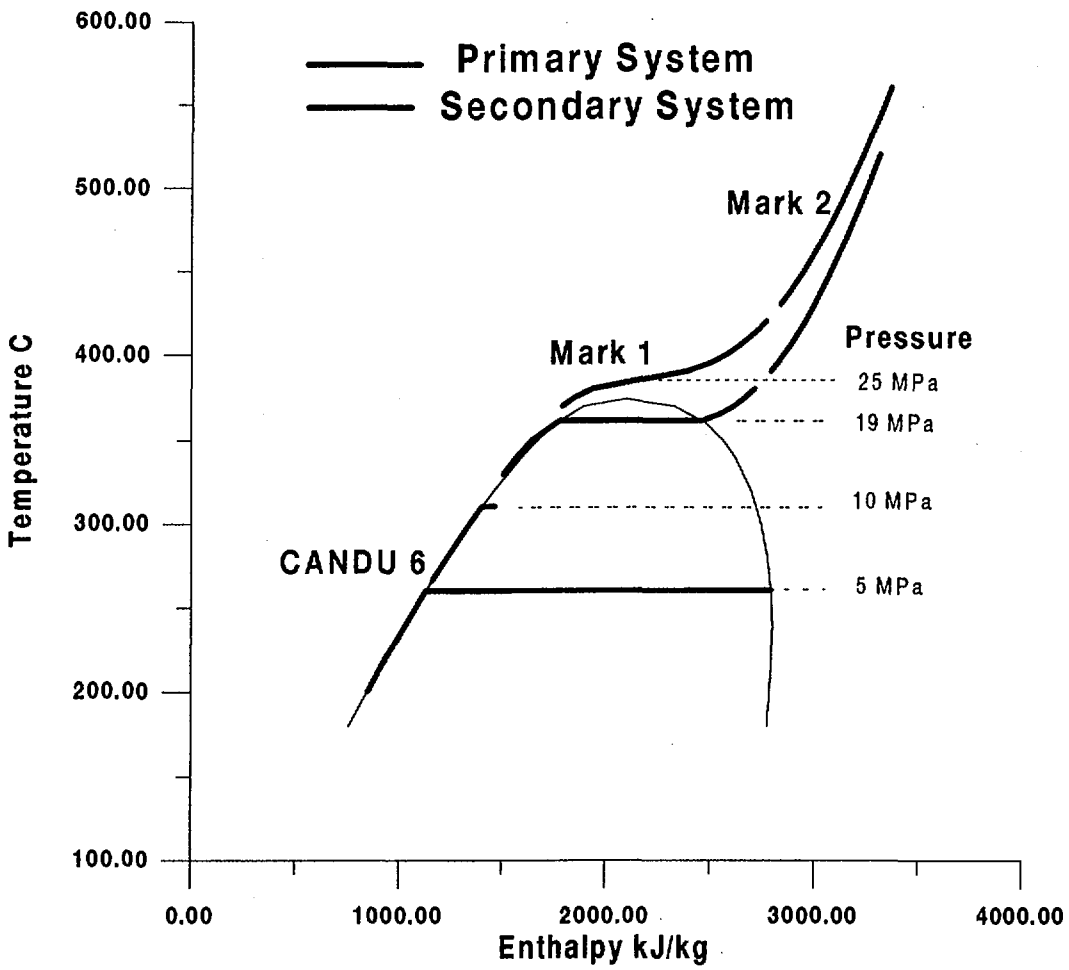

Figure 2: CANDU Evolution to Supercritical Coolant Conditions

Mark 1 Design

The initial calculations for the Mark 1 design were based on heavy water at 25 MPa between 370°C at core inlet and 420°C at core outlet, transferring heat to H_2O at 19 MPa heated from 330°C to 380°C in a once-through counter-current-flow steam generator. These results are reported below. However some advantage in control exists, also discussed below, when the outlet temperatures are increased to 430°C for the core and to 400°C for the steam generator.

Flow, Pressure Drop and Pumping Power

At in-core temperatures around 400°C, i.e. just above the critical temperature of 370°C, the exceptionally high specific heat leads to an attractive heavy-water-cooled design. High specific heat leads to greatly reduced mass flow, pressure drop and pumping power. The enthalpy changes of figure 2 lead to a channel flow 30% of CANDU 6 for the same channel power. Channel pressure drop would be similarly reduced. Primary pumping power would be reduced by factor 6, not only because of the reduced mass flow and pressure drop, but also because of a high coolant density (0.6 g/cc) at the pumps. A rapid density reduction in the core leads to a greatly reduced core-mean density, as discussed below.

Peak Fuel Clad Temperature

High specific heat near the critical point leads to high heat transfer coefficient and modest fuel clad temperatures. These were calculated as follows:
The peak clad temperature was evaluated at the nominal maximum power for a CANDU 6 fuel element and at a coolant temperature of 400°C. From figure 2 it is seen that this temperature will occur at a position towards the outlet end of the channel. The nominal maximum power of 50.7 kW/m for an outer element was taken from a CANDU 6 safety report. Fuel bundle geometric details are for 37 element fuel.

The fuel-to-coolant heat transfer coefficient was calculated using equation 3 of reference 1. The clad to coolant temperature difference is only 50°C, even at the reduced channel flow, leading to a clad nominal maximum temperature of 450°C. Clad corrosion rates should be acceptable at these temperatures, but further investigation is needed on the corrosion and general behaviour of conventional or near-conventional CANDU fuel under such conditions of steam cooling at high pressure and high temperature.

Void Reactivity and Thermodynamic Efficiency

At the Mark 1 temperatures of figure 2, the core-mean coolant density is 0.28 g/cc leading to a heavy-water void reactivity reduced from 15 mk to about 4.5 mk. At the

thermodynamic mean temperature[1] of 360°C on the secondary side of the steam generator, the Carnot efficiency is 1.21 times that of CANDU 6 leading to an 18% cost reduction.

Heavy-Water Inventory and Primary Pressure Control

The coolant core-mean density of 0.28 g/cc could lead to a 70 % reduction of coolant inventory at full power. However, additional heavy water might be needed to fill the PHTS at reduced power, especially in the cold shutdown condition. Two options are discussed below aimed at avoiding such a need and leading to a 3% additional capital cost reduction.

Option 1 Helium

Pressure could be controlled with a helium over heavy water pressurizer as shown in figure 3. On cold shutdown, helium would enter the large piping and steam-generator piping, to accommodate heavy water shrinkage, but there would be sufficient heavy water to fill headers, feeders and fuel channels.

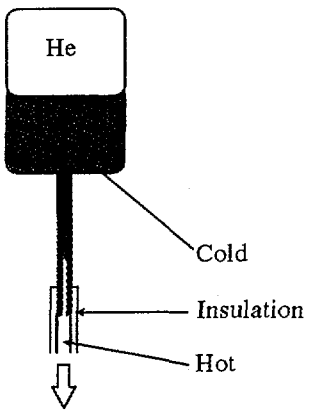

Figure 3: Helium Pressurizer

Start up could be done with nuclear heat or with an external heat source. With nuclear heat, after going critical, the next step would be to raise temperature at low power. As the heavy-water boils at lower pressures, steam and helium would flow to the pressurizer where the steam could be condensed, purging helium from the heat transport system. When operating pressures and temperatures are reached, pumping could start, enabling power to be increased.

[1] Tmean = change-in-enthalpy / change-in-entropy where the changes apply over the secondary side of the steam generator.

A LOCA, during start up, could be problematic. At lower temperatures, the coolant in-core density is high holding up significant reactivity and, at high pressure, a fast blowdown might be expected. Even starting from low power, the rapid rate of insertion of reactivity could lead to an excessive power pulse.

Cool down is envisaged in a reversal of the start up sequence. Thus, at a decay power sufficiently low to permit fuel cooling by hot stagnant supercritical water, pumps could be turned off and cool down commenced via heat transfer to the moderator. A two-phase coolant condition could be avoided by controlling helium pressure to above the saturation pressure. This may be desirable to avoid, for example, stratified flow in horizontal fuel channels.

At the cold shutdown condition, the additional channel coolant inventory would reduce reactivity by some 10 mk but cold start up could always be done with low xenon levels in the core so there would always be plenty of reactivity available. Reactivity would be gained as operating temperatures are reached but would be readily controlled at low power.

High pressure helium control is likely to lead to diffusion of helium into the heavy water coolant with potentially deleterious effects. For example helium is likely to degrade the heat transfer from fuel to coolant. It could also degrade pump performance but this may not be too important for Mark 1 with its modest flow requirements. Loop tests would be needed in any development of this option.

Another difficulty with helium is its containment. The gas is notorious for diffusing through all materials, including metals, and it will tend to leak out of the pressurizer at the high pressures of Mark 1.

Option 2 Heavy Water Transfer Between Moderator and Primary System

This idea is to transfer heavy water from the moderator to the PHTS to accommodate primary system shrinkage during cool-down. It presents problems with tritium releases from higher PHTS tritium levels and with the cost of higher PHTS heavy water isotopic concentration. However the latter could be compensated by the use of a common heavy-water upgrader. Conventional PHTS pH levels are different than that in the moderator in order to control corrosion of carbon steel PHTS piping. However this may not be an issue with Mark 1 because stainless steel ex-core piping is likely needed at the higher coolant temperatures.

A disadvantage with transfer of heavy water from the moderator is impairment of the moderator heat sink. The CANTHERM fuel channel potentially improves the moderator heat sink to the extent that it could provide effective maintenance cooling. With transfer of heavy water to the PHTS, cooling could still be provided but with sprays and reliance on a/c power. Mark 1 would not be passive.

With reduced moderator inventory, the reactor could not be started on nuclear heat. However the PHTS would be full and could be heated on pump heat augmented if necessary by external heaters. The hot heavy water would have to be cooled during transfer to the moderator. Once operating temperatures are attained, the reactor could go critical, pumps started and power raised.

A conventional electrically-heated pressurizer cannot effect much of a change in pressure for water at the outlet temperature of 420°C. However it could be used at 400°C when connected to the inlet header or pump-suction header. With the inlet water at 370°C and the pressurizer set at 400°C, a small change in pressurizer temperature will effect a big change in pressure. The pump-suction header connection is preferred because, in the event of a pump trip, the hot end of the fuel channel would not see additional pressure.

The pressurizer would not have a liquid level to use for inventory control but the temperature itself might be usable. A loss of inventory would reduce the fluid specific volume in the pressurizer which, at constant pressure, requires an increase of temperature. So if the pressurizer temperature increases, add heavy water.

Secondary Pressure and Temperature Control

On the secondary side, pressure control could be done via the usual reactor power or turbine governor-valve control. For the Mark 1 once-through steam generator, in place of conventional boiler level control, feed-water flow could be varied to control the degree of steam superheat thereby maintaining the turbine inlet condition. It is expected that this would lead to a feed-water flow closely proportional to thermal power thereby maintaining a near constant temperature profile on the secondary side of the steam generator.

Primary Flow and Temperature Control

Consider maintaining full primary-side pumping from low to full power and consider permitting primary temperatures to simply follow secondary temperatures.

Figure 4 shows temperature variations in the once-through steam generator. Data are plotted from light-water steam tables for the secondary side at 19 MPa and the primary side at 25 MPa. The primary and steam-generator hot side temperatures are increased somewhat from those considered above. Various primary-side curves are shown in colour with the full-power case shown in red.

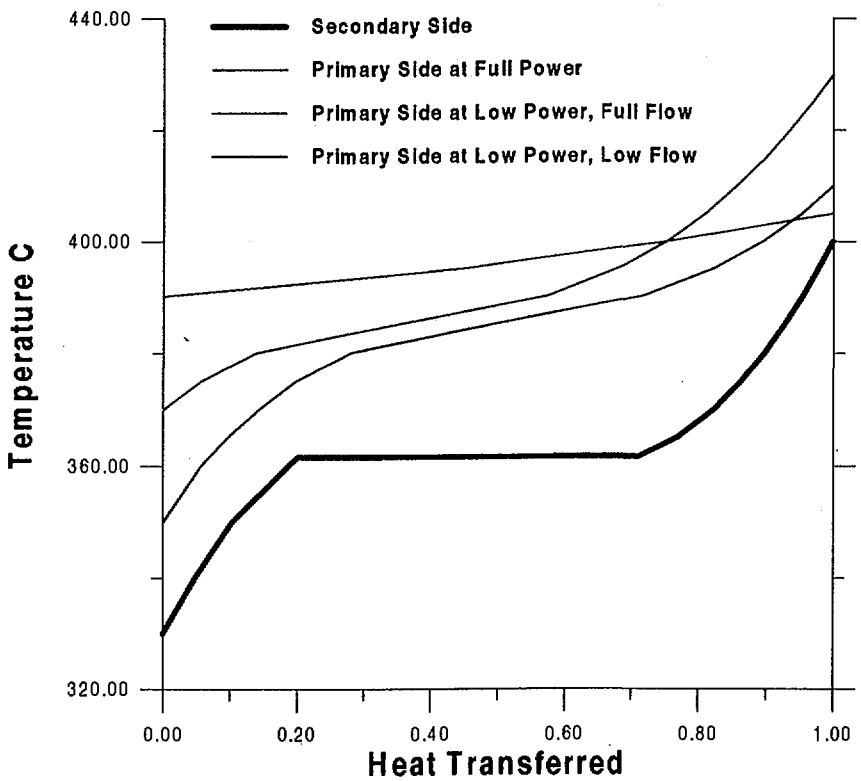

Steam Generator Temperature Distributions
Figure 4

By maintaining full pumping throughout the power range, at low power the entire primary circuit will come to a temperature just above the secondary superheated steam temperature, as shown in the green curve of figure 4. The core-mean coolant temperature at low power will be higher than that at full power and the power to reactivity coefficient from coolant density will be negative in spite of the "positive" void coefficient. On the other hand if flow were made proportional to power, the primary temperatures would be reduced, at low power, as shown in the blue curve of figure 4. This would lead to a larger

coolant inventory at low power and an inventory that would be clearly reducing as power is raised. The power to reactivity coefficient from coolant density would be clearly positive.

Conclusion

A heavy-water-cooled CANDU design at supercritical temperatures and pressures becomes possible with the advanced CANTHERM fuel channel and provides a plant with increased thermodynamic efficiency and reduced coolant density without troublesome two-phase flow phenomena such as fuel dry out and flow instability. The reduced density leads to reduced heavy-water inventory and reduced void reactivity.

A first stage "Mark 1" conceptual design of a supercritical heavy-water-cooled CANDU reactor has been described. The coolant core-mean temperature of about 400°C leads to a reduction in unit energy cost of about 20% compared with conventional CANDU designs. It also leads to a void reactivity reduced by a factor 3 from conventional values. Reduced coolant inventory should result in a further 3% cost reduction. High coolant specific heat leads to a reduced mass flow, again by a factor 3, and a pumping power requirement reduced by factor 6. High coolant specific heat leads to good heat transfer from fuel to coolant, even at the reduced flow, resulting in a peak fuel clad temperature of only 450°C. Mark 1 is expected to be able to use near-conventional CANDU fuel.

Reference

1. Yamagata et al, "Forced Convective Heat Transfer to Supercritical Water Flowing in Tubes", Int. J. Heat Mass Transfer, Vol. 15, 1972.

DYNAMIC SELF-IGNITION OF A FUSION PLASMA

D.R. Kingdon[1], K.F. Schoepf[2], T.K. Hladschik[2], A.A. Harms[1]

[1]Dept. Engineering Physics, McMaster University, Hamilton, Ontario, Canada L8S 4L7
[2]Institute for Theoretical Physics, University of Innsbruck, A-6020 Innsbruck, Austria

ABSTRACT

A new criterion for fusion plasma ignition in d-t tokamaks is established by incorporating non-stationary reaction-thermal dynamics of the plasma into the analysis. Herein the application of a 'soft' Troyon beta limit, together with the actual fusion power deposition and its effect of deteriorating the plasma energy confinement time, are crucial parts of the fusion burn dynamics which determine the ignition conditions. We find that the separatrix established by the dynamic trajectorial evolution of the plasma in the temperature-fuel ion density state plane -- not simply the zero power contour used previously -- is the critical boundary that must be exceeded for the stable ignited operating point to be attained, and maintained, without auxiliary heating.

IGNITION OF A PLASMA

Fusion energy production with tokamak devices demands particular attention to confinement and fuelling regimes that maintain the average fuel ion density $\bar{n}$ and the average plasma temperature $\bar{T}$ at favourable values for optimization of the triple product $\bar{n}\tau_E\bar{T}$, where τ_E denotes the plasma energy confinement time (1). The identification of state and parameter space regions capable of ignited fusion plasma operation is required for significant energy gains to be realized from such systems. This increased energy gain is possible when little or no input power is required to sustain the plasma temperature at a suitable level for fusion reactions to make a useful contribution to the system's energy balance. If ignition is attained, cold fuelling then becomes the sole required injection to the system.

Several definitions of fusion plasma ignition have been considered in the analysis of d-t tokamaks (2,3,4). The requirement that plasma power gains be greater than power losses is consistent, however Ohmic and occasionally auxiliary heating power are included in the power gains. Only Ohmic heating should be so included as the plasma current in a tokamak is always present for plasma stability. While there are numerous references establishing ignited regimes based on steady state power balance calculations, here we consider the non-linear dynamics of the fusion plasma since a steady state power balance alone does not reveal all regions of state space which evolve to the stable ignited operating point.

A globally averaged nonlinear formulation of the dynamic evolutions of density and temperature in an ITER-like d-t tokamak fusion plasma with local temperature T(**r**,t), and local fuel ion density (deuterons plus tritons) n(**r**,t) is considered. These state variables are assumed to take on radial profiles which are constant around the toroid (2):

$$T(r,t) = T_o(t)\left(1 - \frac{r^2}{a^2}\right)^{\gamma_T}, \qquad n(r,t) = n_o(t)\left(1 - \frac{r^2}{a^2}\right)^{\gamma_n}. \tag{1}$$

The peak values of temperature and fuel ion density on the central toroidal axis are $T_o(t)$ and $n_o(t)$ respectively, and r is the radial distance from that axis. The ITER design parameters (5) are used throughout this work; a is the plasma minor radius, $\gamma_T = 1.0$ and $\gamma_n = 0.5$.

REACTION-THERMAL DYNAMICS

The dynamics of plasma fuel ion density evolution are here described on a basis of plasma volume averages by

$$\frac{d\bar{n}}{dt} = \bar{S}(t) - \frac{\bar{n}(t)}{\tau_p} - \frac{1}{2}\overline{\langle\sigma v\rangle_{dt}(r,t)\, n^2(r,t)}\,, \tag{2}$$

where $\bar{S}(t)$ is the volume averaged fuel ion injection rate. The particle confinement time τ_p is taken to be five times the energy confinement time; $\langle\sigma v\rangle_{dt}$ is the d-t fusion reaction rate parameter. The over-line indicates global averaging over the plasma volume throughout this work. Assuming a constant alpha particle impurity density of $0.03\bar{n}$, the average electron density $\bar{n}_e$ is determined by charge conservation.

The global plasma power balance is formulated as

$$\frac{d(\frac{3}{2}\overline{(n_i+n_e)T})}{dt} = \bar{P}_{aux} + \bar{P}_{ohm} - \frac{\frac{3}{2}\overline{(n_i+n_e)T}}{\tau_E} + \eta_\alpha \bar{P}_\alpha - \bar{P}_{brems} - \bar{P}_{cyc}\,, \tag{3}$$

where n_i is the total ion density including the alpha particle impurities, and $\bar{P}_{aux}$ and $\bar{P}_{ohm}$ are the auxiliary and ohmic power densities input to the plasma, respectively. The fraction of the d-t fusion alpha power density, $\bar{P}_\alpha$, retained in the plasma is η_α, while $\bar{P}_{brems}$ and $\bar{P}_{cyc}$ are the bremsstrahlung and cyclotron radiation power density losses from the plasma. Recent analyses of alpha particle thermalization and energy deposition to the plasma (6) revealed a difference of less than 1 keV between the ion and electron temperatures on the time scale of the dynamic (7) unless there is substantial preferential auxiliary heating of one species. Thus, a single temperature formulation was deemed sufficient. Formulations for the terms on the right-hand-side (RHS) of Eq.(3) are as follows, with the power expressions in units of keV·s^{-1}·m^{-3}.

The globally averaged ohmic heating power density due to the induced toroidal plasma current is here taken to be (8)

$$\bar{P}_{ohm} = \frac{1.7\times10^{19} Z_{eff} I^2}{a^4 \kappa^2 \bar{T}^{3/2}}\,, \tag{4}$$

where I is the plasma current (MA), and κ the plasma elipticity (5). The effective charge of the plasma, Z_{eff}, is defined by (1)

$$Z_{eff} = \frac{\sum_j \bar{n}_j Z_j^2}{\bar{n}_e}\,, \tag{5}$$

where $\bar{n}_j$ is the average particle density and Z_j the charge number of the j-th type ion.

The local bremsstrahlung radiation power density losses are (1)

$$P_{brems} = 3.346\times10^{-21} n_e^2 \sqrt{T}\,[Z_{eff}(1+0.00155T+7.15\times10^{-6}T^2) + \frac{0.071C_1}{\sqrt{T}} + 0.00414T\,]\,, \tag{6}$$

where C_1 is a similar quantity to Z_{eff}, the former given by (1)

$$C_1 = \frac{\sum_j \bar{n}_j Z_j^3}{\bar{n}_e} . \tag{7}$$

Local cyclotron radiation losses are taken as (1)

$$P_{cyc} = 0.3878 n_e T B^2 \phi , \tag{8}$$

where B is the toroidal magnetic field (Tesla),

$$\phi = \frac{0.005198}{\sqrt{\Lambda}} T^{3/2} \sqrt{1 + \frac{22.61\, a}{R\sqrt{T}}} \sqrt{1 - R_f} , \tag{9}$$

and

$$\sqrt{\Lambda} = 7.78 \times 10^{-9} \sqrt{\frac{n_e\, a}{B}} . \tag{10}$$

The plasma major radius is R, and R_f is the global cyclotron radiation re-absorption fraction -- taken to be 0.9 herein.

The globally averaged d-t fusion alpha power density is evidently

$$\bar{P}_\alpha = \frac{3517}{4} \overline{\langle \sigma v \rangle_{dt} n^2} . \tag{11}$$

For the global energy confinement time, the ITER scaling law (9)

$$\tau_E = \frac{0.048 f_e \sqrt{\kappa M}\, a^{0.3} R^{1.2} I^{0.85} B^{0.2} \bar{n}_e^{0.1}}{\sqrt{\bar{P}}} , \tag{12}$$

was used, where f_e is the h-mode energy confinement time enhancement factor, M the average isotopic mass of the plasma, $\bar{n}_e$ is in 10^{20} m^{-3}, and $\bar{P}$ the total power (MW) contributing to the degradation of confinement, explicitly:

$$\bar{P} = \bar{P}_{aux} + \bar{P}_{ohm} + f_\alpha \eta_\alpha \bar{P}_\alpha . \tag{13}$$

The fraction of d-t fusion alpha power which degrades confinement is taken here to be $f_\alpha = 0.5$, and further $\eta_\alpha = 0.95$ (6). Combining Eqs.(12) and (13), evaluating the ITER parameters and introducing a soft beta limit (2) yields

$$\tau_E = \frac{1.056 \times 10^9\, \bar{n}_e^{0.1}}{SBL\sqrt{\bar{P}_{aux} + \bar{P}_{ohm} + f_\alpha \eta_\alpha \bar{P}_\alpha}} , \tag{14}$$

with $\bar{n}_e$ now in m^{-3}.

A soft beta limit of the form

$$SBL = e^{\left(\frac{\beta}{0.85\beta_c}\right)^{10}}, \tag{15}$$

was used to model confinement degradation near the Troyon limit, or critical beta

$$\beta_c(\%) = \frac{C_{Troy} I}{aB}, \tag{16}$$

in an inhibitive manner which differs from that found in the literature (2,10). C_{Troy} is the Troyon factor (2). Specifically, confinement degradation was made to begin at ~80% of β_{crit} and increase exponentially such that transport losses were increased by a factor > 10^2 at the Troyon limit. It is expected that such enhanced transport losses will occur due to the increasing kinetic pressure within the tokamak as the beta limit is approached and not only if β_{crit} is surpassed.

CALCULATIONAL ASSESSMENT

Taking the burn characteristics of the d-t fusion plasma as determined by the temporal evolutions of $\bar{n}(t)$ and $\bar{T}(t)$, we examine the associated dynamics in a state plane spanned by the state variables $\bar{T}$ and $\bar{n}$. Two stationary points of the system dynamic (the solution of the RHS of both Eq.(2) and Eq.(3) = 0 with $\bar{P}_{aux}$ = 0) -- one an attractor and the other a saddle point are shown in Figure 1. Also depicted are the regions of the $\bar{T}$-$\bar{n}$ plane for which there is a positive steady state power balance (RHS of Eq.(3) > 0 with $\bar{P}_{aux}$ = 0) -- bounded by the zero power contours, all for an ion injection rate of $\bar{S}$ = 0.05×10^{20} $m^{-3} \cdot s^{-1}$. The latter region is the area of the state plane where the net power deposited in the plasma exceeds the total power losses, and thus where ignited plasma operation would appear possible. The Ohmic ignition point ($\bar{n} > 10^{21}$ m^{-3}) is not shown as it is of no interest here due to the insignificant fusion power.

However, of greater interest is the dynamic evolution of the system determined by solving Eqs.(2) and (3) for $\bar{n}(t)$ and $\bar{T}(t)$, yielding the trajectories and separatrices of Figure 1. Evidently, a high temperature, low density region from which the stable ignited point is attained dynamically exists outside the zero power contours. This region of 'dynamic ignition' is not foreseeable solely through power balance ignition studies, and thus alters the regimes of the $\bar{T}$-$\bar{n}$ state plane which are ignited -- those plasma states which do not require auxiliary heating or control to evolve to, and remain at, the stable high temperature attractor.

Conversely, the region below the separatrix but within the positive steady state power balance region does not ignite as the system's dynamics result in a trajectorial evolution to the low temperature, high density, Ohmic operating point. This further alters the conventional ignited regions of state space, and so the ignition criterion for an ITER-like plasma is not merely achieving a plasma state within the positive steady state power balance region, but rather the separatrix of Figure 1 must be exceeded for the system to evolve dynamically to its high temperature attractor. The location and nature of this attractor has elsewhere been shown (10) to be dependent upon the fuel ion injection rate.

The region of dynamic ignition suggests a possible new approach to heating a fusion plasma to ignited conditions. If attaining a plasma state within this region of state space is less energy demanding than attaining one within the steady state-defined ignition region, a less energy intensive method to achieve plasma ignition is evident.

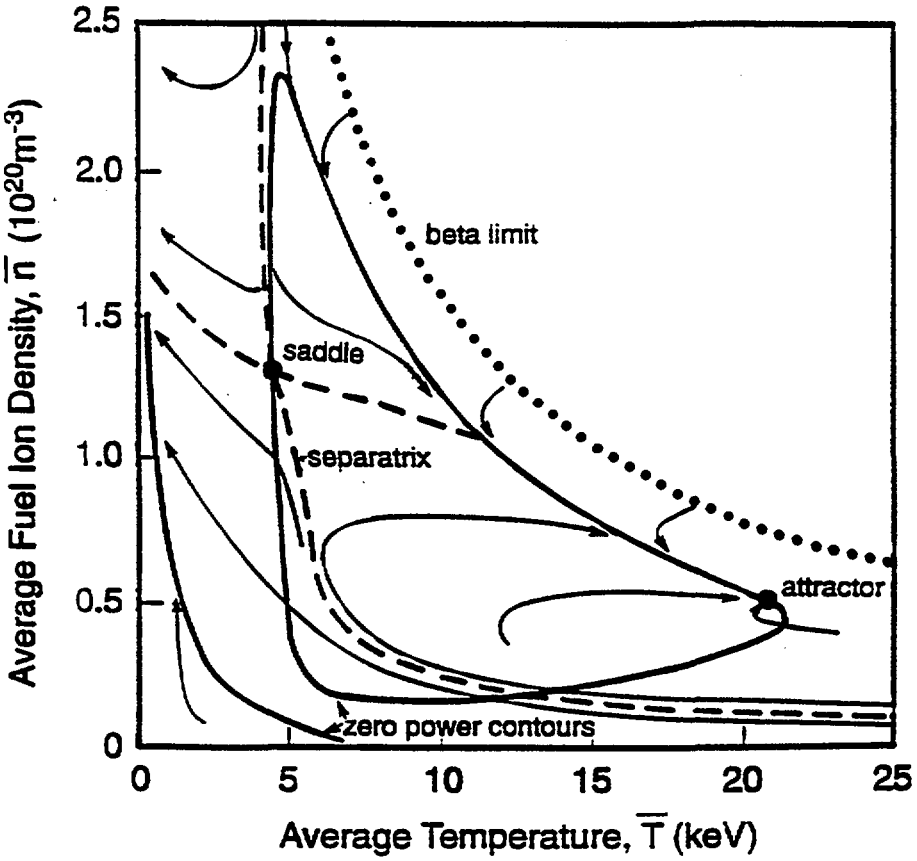

Figure 1: Steady state power balance ignition regimes of the $\bar{T}$-$\bar{n}$ state plane bounded by the zero power contours ($\bar{P}_{aux}$ = 0) and the dynamic ignition regimes defined by the separatrix deduced from state plane trajectories ($\bar{S}$ = 0.05 × 10^{20} m^{-3}·s^{-1}).

CONCLUDING COMMENTS

We thus conclude that the criterion for ignited operation of a fusion plasma is the crossing of the separatrix in the $\bar{T}$-$\bar{n}$ state plane -- a consequence of the non-linear dynamics of the system -- as the power balance alone does not completely reveal which regions of state space evolve dynamically to the stable ignited attractor. A region of 'dynamic self-ignition' outside the positive power balance region was identified and the dynamic ignition criterion of exceeding the separatrix must be recognized as an important consideration for both initial plasma heating and ignited operation of a d-t tokamak.

REFERENCES

(1) McNALLY Jr., J.R., "Physics of Fusion Fuel Cycles", Nuclear Technology/Fusion, Vol. 2, No. 1, p. 9-28, 1982.

(2) ANDERSON, D., T. ELEVANT, H. HAMNEN, M. LISAK, and H. PERSSON, "Studies of Fusion Burn Control", Fusion Technology, Vol. 23, No. 1, p. 5-41, 1993.

(3) SCHOEPF, K.F., and T. HLADSCHIK, "Dynamic Ignition - A New Operation Criterion For Fusion Plasmas", Annals of Nuclear Energy, Vol. 23, No. 1, p. 59-64, 1996.

(4) VOLD, E.L., T.K. MAU, and R.W. CONN, "Tokamak Power Reactor Ignition and Time-Dependent Fractional Power Operation", Fusion Technology, Vol. 12, No. 2, p. 197-229, 1987.

(5) UCKAN, N.A., J. HOGAN, W. HOULBERG, J. GALAMBOS, L.J. PERKINS, S. HANEY, D. POST, and S. KAYE, "ITER Design: Physics Basis for Size, Confinement Capability, Power Levels and Burn Control", Fusion Technology, Vol. 26, No. 3, p. 327-330, 1994.

(6) HLADSCHIK, T.K., and K.F. SCHOEPF, "TF-Ripple Loss Effects on Fusion Alpha Heating", Fusion Technology, Vol. 26, No. 3, p. 588-592, 1994.

(7) HLADSCHIK, T.K., "Reactor Physics Investigations of the ITER Fusion Dynamic" (in German), PhD Dissertation, University of Innsbruck, Innsbruck, Austria, June 1994.

(8) JOHNER, J., "Thermonuclear Ignition in the Next-Generation Tokamaks", Fusion Technology, Vol. 19, No. 3, p. 515-530, 1991.

(9) YUSHMANOV, P.N., T. TAKIZUKA, K.S. REIDEL, O.J.W.F. KARDAUN, J.G. CORDEY, S.M. KAYE, and D.E. POST, "Scalings for Tokamak Energy Confinement", Nuclear Fusion, Vol. 30, No. 10, p. 1999-2006, 1990.

(10) SCHOEPF, K., B. HEUSCHNEIDER, and T. HLADSCHIK, "Nonlinear Fusion Dynamics in d-t Tokamak Plasmas", Kerntechnik, Vol. 60, No. 4, 179-184, 1995.

CNS Technical Program

MONDAY, 1997 June 9

Session 1D Health and Biology Eglington Room

Chair: D. Whillans
Ontario Hydro

14:00-14:25 *Canadian and United States Regulatory Models Compared: Doses from Atmospheric Pathways*
by S.-R. Peterson (Atomic Energy of Canada Limited)

14:25-14:50 *Establishing Credibility in the Environmental Models Used for Safety and Licensing Calculations in the Nuclear Industry*
by P.A. Davis (Atomic Energy of Canada Limited)

14:50-15:15 *Report on the Recently-Updated Study of Cancer Mortality in the A-Bomb Survivors: Insights for Radiation Protection*
by N.E. Gentner (Atomic Energy of Canada Limited)

15:15-15:45 Break

15:45-16:10 *Tritium Beta-Radiation Induction of Chromosomal Damage: A Calibration Curve for Low-Dose, Low-Dose-Rate Exposures of Human Cells to Tritiated Water*
by D.P. Morrison, K.L. Gale (Atomic Energy of Canada Limited), and J.N. Lucas, F.S. Hill, T. Straume (University of California and Lawrence Livermore Laboratory)

16:10-16:35 *The RBE of Tritium-Beta Exposure for the Induction of the Adaptive Response and Apoptosis; Cellular Defense Mechanisms Against the Biological Effects of Ionizing Radiation*
by D.R. Boreham, M.E. Bahen, J.-A. Dolling, R.E.J. Mitchel (Atomic Energy of Canada Limited)

16:35-17:00 *Lung Cancer and Inhaled Uranium Ore Dust in Rats*
by R.E.J. Mitchel, J.S. Jackson (Atomic Energy of Canada Limited)

CANADIAN AND UNITED STATES REGULATORY MODELS COMPARED: DOSES FROM ATMOSPHERIC PATHWAYS

S-R. Peterson
Research Officer
Atomic Energy of Canada Limited
Chalk River, Ontario

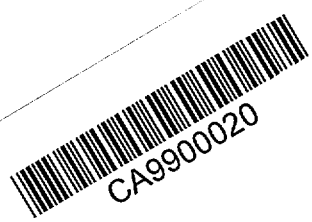

INTRODUCTION

CANDU reactors sold offshore are licensed primarily to satisfy Canadian regulations. For radioactive emissions during normal operation, the Canadian Standards Association's CAN/CSA-N288.1-M87 (1) is used. This standard provides guidelines and methodologies for calculating a rate of radionuclide release that exposes a member of the public to the annual dose limit.

In some countries such as the Republic of Korea, the regulatory requirement is to calculate the annual dose to members of the critical group. To calculate doses from air concentrations, either CSA-N288.1 or the Regulatory Guide 1.109 (2) of the United States Nuclear Regulatory Commission, which has already been used to license light-water reactors in these countries, may be used. When dose predictions from CSA-N288.1 (called CSA henceforth) are compared with those from the U. S. Regulatory Guides (called RG henceforth), the differences in projected doses raise questions about the predictions. This report explains differences between the two models for ingestion, inhalation, external and immersion doses.

For compliance with nuclear regulations, emissions reported in terms of percent DRLs for CANDU reactors routinely include tritium, ^{14}C, noble gases (as Bq MeV), radioiodine (as ^{131}I) and unidentified particulates. Stack sampling provides supporting numbers during operation to a greater or lesser extent. In addition, at some sites and under some conditions, measured or estimated releases are available for other radionuclides (3, 4, 5, 6, 7). There are no data for a number of radionuclides, and many of the particulate values are single measurements or even estimates (3). These data, adjusted as emissions from a single CANDU reactor unit and averaged with extremes discarded (Table 1) are used here to calculate doses from unit releases and actual releases for both models.

Table 1
Radionuclides Released from CANDUs and Average Measured and Assumed Source Terms

	Average Measurements Bq s^{-1}	Assumptions Bq s^{-1}
H-3	7.0E+06	
C-14	1.4E+04	
Cr-51		7.1E-02
Mn-54		7.1E-02
Fe-59	2.0E-03	
Co-58	1.4E-03	
Co-60	2.3E-02	
Zn-65		7.1E-02
Sr-89		7.1E-02
Sr-90		7.1E-02
Zr-95	1.5E-01	
Nb-95	1.7E-01	
Mo-99	3.3E-03	
Ru-103		7.1E-02
Ru-106	4.6E-02	
Te-132	1.6E-03	
I-131	3.1E-01	
I-132	4.5E-01	
I-133	6.2E-01	
I-134	6.3E-01	
I-135	5.6E-01	
Cs-134	9.9E-02	
Cs-136	6.5E-03	
Cs-137	2.7E-01	
Ba-140		7.1E-02
Ce-141		7.1E-02
Ce-144		7.1E-02
Ar-41	1.5E+05	
Kr-85m	5.3E+04	
Kr-87	9.6E+04	
Kr-88	2.7E+05	
Xe-133	3.9E+06	
Xe-135	6.3E+05	

DOSES

Ingestion Pathways

In addition to real differences between the models which are due primarily to differences in parameter values, significant differences will arise because of assumptions made by the user. The aim in this intercomparison is to assure that assumptions made by the user apply equally to both models.

Assumptions Made for Comparison. The endpoints for concentrations in foodstuffs and ingestion doses are different for RG and CSA because of different definitions of vegetables and meat and different diets (Table 2). Consequently, the models should not be compared directly and nevertheless, meaningful comparison is possible if certain assumptions are made.

Table 2
Important Differences in Parameters and Model Assumptions for Rg 1.109 and CSA-N288.1

Consumption for adults and infants in kg per annum assumed

	RG* Adult	CSA** Adult	RG* Infant	CSA** Infant
Leafy vegetables	64	14		10
Fruit vegetables	108.4	55		25
Root vegetables	108.4	79		24
Fruit	114.4	55		25
Grain	124.8	[74]		[12]
Milk & milk products	310	174	330	220
Beef (meat)	110	35.5		12
Pork		35.5		12
Poultry		16		10
Eggs		14		5

* Recommended values for intake to be used for the maximum exposed individual in lieu of site-specific data RG groups fruits, vegetables, and grain: 520 kg per annum; leafy vegetable, 64 kg per annum Consumption of vegetables products defined: (on a mass basis) 22% fruit, 54% vegetables (including leafy) and 24% grain.

** Recommended average food consumption rates in lieu of site-specific data; CSA groups above-ground vegetables (fruit vegetables) and fruit, 110 kg for adult, 50 kg for infant; beef and pork, 71 kg for adult, 24 kg for infant. Numbers in square brackets are shown for diet with no guidance for how to calculate concentrations.

Days to ingestion in RG (0 days to ingestion in CSA):

Leafy vegetables	1 d to maximally exposed individual
Produce	60 d to maximally exposed individual
Unspecified vegetables	14 d to member of the general population
Milk	2 d to maximally exposed individual
Milk	4 d to member of the general population
Meat	20 days from slaughter to consumption

Fraction of food arising from a contaminated source

	CSA	RG
Leafy veg	site specific	1
Produce	site specific	0.76

In RG the following delays apply:

Pasture	0 days (assumed here for comparison)
Hay	90 days if stored

Period of long term build up in the soil in years based on lifetime of power station

RG	CSA
15	infinite

The assumptions made for this intercomparison included:

- Air concentrations at 1000 m from the elevated source are 5.4 10^{-7} Bq m^{-3}.
- The member of the critical group for whom all doses are calculated lives 1000 m from the source and is self-sufficient, i.e., raising all necessary food for a completely contaminated diet.
- For tritium, the ratio of the tritium in the plant to the tritium in the air is set at 0.5 with an absolute humidity of 0.01 kg m^{-3} for RG. This corresponds to the CSA default value of 50 m^3 kg^{-1} for the transfer from air to vegetation.
- For carbon, there are 0.16 g carbon per cubic meter of air.
- For comparison between RG and CSA, the minimum time between harvest and ingestion in RG was assumed: 1 day for all vegetables, 2 days for milk, 20 days for meat.
- When vegetable crop concentrations are compared, the single RG value is compared with a weighted average of the concentrations of CSA's four different crops based on annual adult intake of each.
- Meat concentrations from RG are compared with a weighted average of beef, pork, poultry and eggs based on annual adult intake of each in CSA.
- In CSA, it is assumed that all feed consumed by animals is equivalent to eating off pasture all year, unless the radionuclide is short-lived (< 1 month), in which case a winter non-grazing factor of 0.5 is introduced. In RG, the user can select fractions of pasture or hay that has been stored for 90 days. In order to compare the models, the RG equation for pasture was modified to account for the winter non-grazing factor for short-lived nuclides, just as in CSA.
- In RG, iodine is considered to be 50% elemental, and only this portion of the iodine released enters the food chain. In CSA, the released iodine can be fractionated between elemental, particulate and organic fractions. Since particulate iodine also deposits significantly and enters the food chain, for CSA it was assumed that the fractionation is 50% elemental, 25% particulate and 25% organic.
- No wet deposition was considered for either model.
- A factor of 5 was assumed to convert dry weight to fresh weight pasture. RG parameter values are exclusively fresh weight, but CSA forage is in dry weight. Thus CSA values had to be converted to be comparable for the discussion.

Total activity ingested per year per radionuclide is compared for the default diets of each model. However, since these diets are intended to be different (RG's maximal and CSA's average), a better comparison of ingestion dose is made with both models

using the average diet described in CSA. Furthermore, since delays to ingestion in RG reduce dose from short-lived radionuclides drastically, the CSA predictions were modified on a spreadsheet to reflect the same delays and to be comparable with RG's (with CSA diet).

Comparison of concentrations in foodstuffs: To understand why ingestion doses differ, it is imperative to compare all the steps from air concentration to concentrations in forage and vegetables to concentrations in milk and meat products and to compare intake from overall diet.

In Table 3, ratios of predicted CSA concentrations divided by RG concentrations (CSA/RG) for pasture, vegetables, milk, beef and meat are compared. Pasture concentrations for CSA are consistently lower than RG's with the exception of ^{90}Sr, which has the highest soil to plant concentration ratio (CR) of the CSA nuclides. CSA's low predictions are due to the difference in yield of the two models: RG's is 0.7 kg, while CSA's is 1.4 kg (recommended generic value in fresh weight). CSA/RG ratios for vegetables mostly lie between 2.4 and 2.6. This is largely due to the lower average yield (1.3 kg m^{-2}) of CSA compared with RG's 2.0 kg fw m^{-2}. The ratios for the shorter-lived iodines, particularly ^{132}I and ^{134}I, are remarkable exceptions. These high ratios (e.g., 4.1 10^8 for ^{134}I) illustrate how important the day's delay to ingestion is for short-lived radionuclides, since when the two results are compared once CSA's have been adjusted for the delay, the ^{134}I ratio falls to 1.9, which agrees with all the other radioiodines.

For tritium, the CSA/RG ratio for concentration in fresh weight pasture is 1.3, like the vegetables. However, there is a conceptual error in CSA's treatment of the specific activity model for tritium. With the specific activity model for tritium, by definition, concentrations of tritium should be calculated on a fresh weight basis, but, in CSA, pasture is given as dry weight. Thus a calculated fresh weight concentration is defined as a dry weight quantity. In practice, either the pasture will have been dried to hay from which essentially all water (including HTO) has been evaporated, and consequently the concentration of HTO in dry weight pasture will be little or nothing, or the calculated tritium concentration in pasture must be expressed in fresh weight. This error affects concentrations of tritium in milk and meat and ultimately ingestion dose from tritium. That CSA's plant concentrations are 30% higher than RG's is due mostly to RG's assumption that 75% of the total plant is water (CSA tacitly assumes 100%).

Table 3
CSA/RG Ratios for Concentrations in Pasture*, Vegetables**, milk and Beef and Meat***

Columns labelled "no delay" compare CSA and RG as calculated by the model; columns labelled "delay" mean the CSA value has been delayed for x days to be comparable to the RG value which is based on time between harvest and ingestion

	Pasture	Vegetables		Milk		Beef		Meat	
		No delay	1 d delay	No delay	2 d delay	No delay	20 d delay	No delay	20 d delay
H-3	1.3	1.3	1.3	0.58	0.58	0.47	0.46	0.63	0.63
C-14	0.80	0.54	0.54	1.0	1.0	1.7	1.7	1.4	1.4
Cr-51	0.40	2.5	2.5	0.20	0.19	2.3	1.4	0.81	0.49
Mn-54	0.40	2.4	2.4	0.54	0.53	0.26	0.25	0.39	0.37
Fe-59	0.46	2.5	2.5	0.11	0.10	0.33	0.24	0.22	0.16
Co-58	0.49	2.6	2.5	1.4	1.4	0.45	0.37	1.4	1.1
Co-60	0.51	2.5	2.5	1.5	1.5	0.40	0.40	1.2	1.2
Zn-65	0.45	2.0	2.0	0.12	0.12	1.6	1.5	1.0	0.97
Sr-89	0.48	2.6	2.5	0.86	0.84	0.84	0.65	5.1	3.9
Sr-90	1.1	2.5	2.5	1.9	1.9	1.4	1.4	8.7	8.7
Zr-95	0.40	2.5	2.5	3.6	3.6	0.33	0.27	0.33	0.27
Nb-95	0.45	2.5	2.5	3.8	3.6	0.60	0.41	0.21	0.22
Mo-99	0.40	3.1	2.4	0.032	0.020	13	0.087	9.2	0.063
Ru-103	0.46	2.5	2.5	1.6	1.6	0.0033	0.0023	0.0024	0.0013
Ru-106	0.50	2.4	2.4	1.7	1.7	0.0026	0.0025	0.0019	0.0014
Te-132	0.39	2.9	2.3	1.4	0.92	13	0.18	11	3.9
I-131	0.32	2.1	1.9	0.62	0.52	2.2	0.39	3.5	0.64
I-132#	0.31	2.6E+03	1.9	1.2E+06	0.63	2.7E+62	0.41	4.6E+62	0.69
I-133#	0.31	4.2	1.9	2.6	0.52	2.9E+06	0.35	4.7E+06	0.57
I-134#	0.31	4.1E+08	1.9	3.9E+16	0.82	2.4E+166	0.45	4.3E+166	0.81
I-135#	0.31	23	1.9	79	0.55	1.5E+21	0.39	2.4E+21	0.65
Cs-134	0.52	2.5	2.5	0.30	0.30	3.4	3.3	5.7	5.5
Cs-136	0.42	2.6	2.5	0.21	0.19	5.9	2.0	9.9	3.4
Cs-137	0.54	2.4	2.4	0.32	0.32	3.5	3.5	5.9	5.9
Ba-140	0.42	2.6	2.5	0.42	0.38	0.038	0.013	0.58	0.31
Ce-141	0.46	2.6	2.5	0.51	0.49	1.4	0.93	0.72	0.47
Ce-144	0.51	2.6	2.6	0.48	0.48	1.0	0.99	0.52	0.50

* Pasture is compared on a fresh weight basis
** The number used for CSA is a weighted average of vegetable and fruit concentrations based on yearly adult diet
*** The number used for CSA is a weighted average of all meats and eggs based on yearly adult intake
# Meaningless high ratios for radionuclides with half-lives less than 1 day show assumption of instantaneous ingestion to be unrealistic

CSA/RG ratios for ^{14}C in pasture and vegetables are also different even though the specific activity model is used in both models. RG has the same ^{14}C concentrations in pasture as in vegetables because all plants are assumed to have 110 g of carbon per kilogram of plant. In contrast, CSA assumes a carbon content of 60 g kg^{-1} vegetable and 440 g kg^{-1} pasture dry weight (equivalent to 88 g if fresh weight). Thus the CSA/RG ratio is slightly higher for pasture than for vegetables. CSA concentrations are lower than RG's because of the assumptions of lower carbon content in fresh weight plants.

In Table 3, concentrations are compared also for milk, beef and "meat" based on weighted averages of meat concentrations from an adult diet. A small contribution to concentration in CSA comes from the inhalation pathway to animals, which is not included in RG.

The CSA/RG ratio for milk averages about 1.0 with about half of the ratios less than 1.0. Since the intake of cows is essentially the same in both models (10 kg dw in CSA and 50 kg fw in RG) most of the difference in milk concentrations can be traced to the lower concentrations found in CSA forage which are not offset by the generally higher forage to milk transfer factors (F_m) in CSA or perhaps are made lower by CSA/RG F_m ratios of less than 1. In both models, both tritium and ^{14}C are calculated using F_m. For tritium, due to the conceptual error in CSA, the cow will ingest 10 kg of dry weight hay with a concentration calculated on the basis of fresh weight. This either overestimates the amount of tritium ingested (i.e., if the hay is dry and free of HTO) or underestimates the amount of tritium ingested by a factor of five (50 kg fresh weight is the equivalent of 10 kg dry weight). Conservatively assuming a fresh weight diet, the CSA/RG ratio for concentration in milk should be 1.9.

The "meat" in RG is supposed to include a diet of meat (unspecified) and poultry, but, the forage to meat transfer factors (F_f) used in RG are more similar to the values used in CSA for beef than they are for the pork, poultry or egg F_f values in CSA. Thus the CSA results (with delays to ingestion) are compared just for beef and for a weighted meat, as mentioned above. For the beef comparison, most ratios are within a factor of 4 except for ^{103}Ru, ^{106}Ru and ^{140}Ba, which are extremely low. If the differences in pasture concentrations were considered, the CSA value would rise by a factor of two, improving the underpredictions and raising the overpredictions. On average, when CSA weighted meat is compared with RG meat, the ratio rises by nearly a factor of two, and the ^{140}Ba CSA value then falls within a factor of three of the RG value. The rutheniums remain

a problem due to the very low F_f for ruthenium in CSA (0.002 d kg^{-1} beef) compared with RG (0.4 d kg^{-1} meat).

Comparison of total diets: CSA/RG ratios are shown in Table 4 for adult and infant. Values compared are for the RG maximal adult diet or milk infant diet, the CSA diet used in RG, the CSA diet in CSA without delay corrections and the CSA diet in CSA with losses due to delays included. The contribution of each radionuclide to adult and infant CSA diets is remarkably similar (within a factor of 2) for CSA and RG. The CSA diet contributes slightly more Becquerels per annum per unit release than does RG because of higher vegetable concentrations than found in RG, which compensate for comparatively lower concentrations in milk and meat. This is true for the infant (CSA diet) too. CSA/RG ratios would be much greater for ^{51}Cr and ^{95}Zr if the CSA diet had included contributions from pork, poultry and eggs not calculated in CSA; similarly, CSA/RG ratios for ^{95}Nb, ^{99}Mo, ^{132}Te, and ^{140}Ba would be somewhat higher if the dietary contribution from pork were calculated in CSA, which it is not. For both adult and infant, the very low ^{103}Ru and ^{106}Ru ratios in the diet are accounted for by extraordinarily low concentrations in meat in CSA. Zinc-65 activity in infant's diets is low because of low concentrations of ^{65}Zn in milk (due to a low F_m) relative to RG. Niobium-95 is a bit low in CSA for the adult diet due to low concentrations in poultry and eggs.

The all milk diet in RG for infants creates some very high CSA/RG ratios, since many radionuclides are not easily transferred to milk compared with other food stuffs. In RG, milk always has the lowest concentration of vegetables, milk and meat. For CSA on average, it ranks 7 out of 9 foodstuffs, and, on average, has a similar concentration to that calculated in RG. For example, in both RG and CSA, very little ruthenium is concentrated in milk. In a total CSA infant diet, between the vegetables and meat, however, there is a lot of ruthenium concentrated, relatively. Thus for annual diet, the CSA/RG-with-milk-diet ratio is 5900 for ^{106}Ru, while the CSA/RG-with-CSA-diet ratio is only 0.12 due to the higher meat concentrations in NUREG compared with CSA.

Quantities of tritium and ^{14}C in diets of adults and infants are essentially the same for the two models.

Ingestion Doses: CSA/RG ratios are shown in Table 5 for adults and infants respectively. All comparisons are based on the use of the CSA diet in both models with delays to ingestion accounted for. For the critical organ comparisons, the highest doses from each model are compared with each other, regardless of whether the dose is highest by being the only dose (i.e., the effective dose in CSA when there is no critical organ). Also, a set of

Table 4
CSA/RG Ratios for Annual Diet for Adult and Infant

ADULT					INFANT				
Nuclide			Decay corrected		Nuclide			Decay corrected	
	Default diet	CSA diet	Default diet	CSA diet		Milk diet	CSA diet	Milk diet	CSA diet
H-3	0.48	0.84	0.48	0.84	H-3	1.2	0.84	1.2	0.84
C-14	0.49	0.80	0.49	0.80	C-14	1.3	0.90	1.3	0.90
Cr-51	0.91	1.7	0.88	1.6	Cr-51	4.7	1.8	4.6	1.7
Mn-54	0.93	1.7	0.92	1.7	Mn-54	24	2.1	23	2.1
Fe-59	0.61	0.88	0.58	0.83	Fe-59	5.4	0.96	5.2	0.92
Co-58	0.96	1.6	0.92	1.5	Co-58	7.8	1.8	7.6	1.7
Co-60	0.92	1.5	0.92	1.5	Co-60	8.1	1.7	8.1	1.7
Zn-65	0.38	0.62	0.37	0.60	Zn-65	0.30	0.37	0.30	0.36
Sr-89	1.0	1.9	0.98	1.8	Sr-89	8.0	2.2	7.9	2.1
Sr-90	1.1	2.0	1.1	2.0	Sr-90	9.8	2.3	9.8	2.3
Zr-95	0.61	0.88	0.60	0.86	Zr-95	1.2E+03	1.0	1.2E+03	1.0
Nb-95	0.37	0.44	0.32	0.38	Nb-95	6.5	0.59	5.8	0.53
Mo-99	0.65	1.2	0.49	0.90	Mo-99	0.57	0.67	0.43	0.51
Ru-103	0.12	0.13	0.11	0.13	Ru-103	5.7E+03	0.16	5.6E+03	0.15
Ru-106	0.09	0.11	0.09	0.11	Ru-106	5.9E+03	0.12	5.9E+03	0.12
Te-132	1.1	2.1	0.90	1.7	Te-132	1.6E+02	2.7	1.3E+02	2.2
I-131	0.74	1.4	0.66	1.2	I-131	1.9	1.4	1.7	1.2
I-132	1.2E+03	2.2E+03	0.74	1.4	I-132	3.2E+06	3.4E+03	1.7E+03	1.8
I-133	1.7	3.1	0.69	1.3	I-133	7.8	3.6	3.0	1.4
I-134	1.9E+08	3.6E+08	0.75	1.4	I-134	8.5E+16	5.8E+08	2.6E+08	1.8
I-135	10.	19.	0.74	1.4	I-135	2.3E+02	26	15	1.7
Cs-134	0.84	1.5	0.84	1.5	Cs-134	0.92	1.0	0.92	1.0
Cs-136	0.82	1.5	0.68	1.2	Cs-136	0.97	1.0	0.80	0.84
Cs-137	0.83	1.5	0.83	1.5	Cs-137	0.93	1.0	0.93	1.0
Ba-140	1.0	1.9	0.94	1.7	Ba-140	28	2.3	26	2.2
Ce-141	0.99	1.8	0.96	1.8	Ce-141	57	2.3	56	2.2
Ce-144	0.98	1.8	0.98	1.8	Ce-144	61	2.3	61	2.3

Table 5
CSA/RG Ratios of Ingestion Dose for Adults

	ADULT					INFANT			
	Total Body		Critical Organ*			Total Body		Critical Organ*	
Nuclide	CRL DCF		CRL DCF		Nuclide	CRL DCF		CRL DCF	
H-3	0.60	0.54	0.60	**0.54**	H-3	0.58	0.48	0.58	**0.48**
C-14	2.7	3.0	0.54	**0.60**	C-14	1.1	1.1	0.22	**0.22**
Cr-51	75	87	0.30	**2.6**	Cr-51	31	1.0E+2	1.1	**28**
Mn-54	4.7	5.2	0.29	**1.0**	Mn-54	1.5	5.4	0.34	**3.4**
Fe-59	1.4	1.4	0.16	**0.76**	Fe-59	0.72	2.08	0.28	**3.1**
Co-58	4.7	2.5	0.52	**1.2**	Co-58	2.7	3.2	2.7	**14**
Co-60	20	3.9	2.3	**1.8**	Co-60	8.9	6.7	8.8	**14**
Zn-65	1.3	1.3	0.58	**0.73**	Zn-65	0.46	0.73	0.21	**0.38**
Sr-89	1.9	2.0	0.05	**0.46**	Sr-89	2.0	2.0	0.056	**0.44**
Sr-90	0.13	0.11	**0.35**	**0.37**	Sr-90	0.44	0.13	0.11	**0.61**
Zr-95	4.3E+2	4.6E+2	1.6	**14**	Zr-95	1.3E+2	6.0E+2	0.18	**7.3**
Nb-95	1.1E+3	4.4E+2	2.4	**6.3**	Nb-95	1.1E+3	6.3E+2	11	**3.0**
Mo-99	5.7	2.5	**4.7**	**10**	Mo-99	1.0	0.97	0.13	**0.79**
Ru-103	4.5	4.5	0.02	**0.15**	Ru-103	1.1	5.2	**0.031**	**1.3**
Ru-106	8.3	7.9	0.02	**0.16**	Ru-106	2.3	7.4	0.04	**1.2**
Te-132	11	10	**5.4**	**1.1E+02**	Te-132	17	13	**72**	**69**
I-131	15	29	**32**	**38**	I-131	21	43	**0.92**	**1.1**
I-132	3.5	7.9	**0.93**	**0.95**	I-132	5.5	13	**1.20**	**1.5**
I-133	14	27	**33**	**40**	I-133	18	43	**0.97**	**1.3**
I-134	1.6	5.5	**0.69**	**0.58**	I-134	7.7	7.7	**1.1**	**0.90**
I-135	6.1	11	**1.0**	**1.1**	I-135	10	21	**1.3**	**1.7**
Cs-134	0.91	0.86	0.74	**0.85**	Cs-134	0.89	0.84	0.090	**0.079**
Cs-136	0.78	NA	0.56	**NA**	Cs-136	0.50	NA	0.19	**NA**
Cs-137	1.1	0.99	0.70	**0.75**	Cs-137	1.2	1.0	0.09	**0.07**
Ba-140	12	13	**4.0**	**4.3**	Ba-140	2.6	16	0.13	**8.4**
Ce-141	7.1E+3	6.5E+3	**2.4**	**2.4**	Ce-141	1.6E+3	7.5E+3	0.37	**20**
Ce-144	1.5E+3	1.3E+3	**2.7**	**2.7**	Ce-144	4.0E+2	2.0E+3	0.39	**23**

* Numbers in bold are the comparisons of critical organ to critical organ; all other comparisons are CSA effective dose/RG dose to critical organ.

revised CSA predictions using updated DCFs (8)compiled for newly calculated DRLs at Chalk River (9) are compared with RG.

For adult effective dose, the CSA/CRL predictions are always higher than or equal to RG's with the exception of tritium, ^{90}Sr, ^{134}Cs and ^{137}Cs. Doses from ^{51}Cr, ^{60}Co, ^{95}Zr, ^{95}Nb, ^{141}Ce and ^{144}Ce are greater (sometimes by an enormous amount) by at least a factor of 20. For dose to a critical organ for an adult, when the CSA value is based on a DCF for effective dose, the CSA predictions are low (very low in the case of ^{89}Sr, ^{103}Ru and ^{106}Ru) or not significantly higher than RG's. When critical organ doses are compared for adults, CSA doses are either equal to or higher than RG's except for ^{90}Sr (0.35), ^{132}I (0.93) and ^{134}I (0.69). For the comparison of critical doses for adults with updated DCFs for CSA, the results are evenly divided between CSA/RG ratios greater than and less than one.

For infants, for the CSA diet, the trend in effective doses is quite similar to that for adults. In a critical organ to critical organ comparison for radioiodines, the CSA/RG ratio is about one. When CSA predictions with new DCFs are compared with RG's, most notable are the very low CSA/RG ratios for the cesiums and the higher ratios for the ceriums.

For tritium, the total body and critical organ doses for adults and infants for CSA are lower than RG's, and the new DCFs lower them a little more, to about half. For ^{14}C, the CSA effective doses for adults and infants are higher than RG's, but CSA doses to critical organ are lower than RG's. The new DCFs raise the dose to critical organ for an adult predicted by CSA to 60% that of RG but leave the predicted infant dose to critical organ at 22%, suggesting that the RG critical organ doses are obsolete.

One major difference between CSA and RG which impacts on ingestion doses is that RG has different DCFs for all critical organs considered, with the exception of tritium where all organs have the same DCF as the total body. Since DCFs to critical organs are higher than DCFs to whole body, the doses to critical organs in RG will invariably be higher than those calculated for total body in CSA (The DCFs for total body in CSA are mostly comparable to or higher than RG's). When DCFs for critical organs are specified in CSA, the organ doses are comparable to RG. The updated DCFs used in CSA are for a complete set of critical organs, and consequently the CSA-CRL/RG ratios are higher than the CSA/RG ratios for doses to critical organs for 80% of the radionuclides.

In a model intercomparison, there can be no right or wrong answers. From experience gained from model testing (10, 11) two similar models with similar assumptions would be expected to

produce similar results, certainly within a factor of +/- 3. The reasons for large deviations from this factor should be examined. Each model has some conservativeness built in: for RG, it is the maximal diet, while for CSA, it is having no delay times to ingestion. Both models employ sets of transfer parameters that are believed to be conservative (hence much of the similarity). Only those doses that differ significantly are cause for concern and should prompt an investigation of both models. Extreme differences between the two models' dose predictions can be explained primarily on the basis of differences in DCFs coupled with smaller differences in dietary contributions.

Inhalation Pathways

The equations for modelling dose from inhalation are essentially the same in CSA and RG, since, although CSA has an occupancy factor not found in RG, the default value is 1. Breathing rates for adults are slightly different: CSA's is 8400 m^3 a^{-1}, and RG's is 8000 m^3 a^{-1}. For infants the breathing rates are identical: 1400 m^3 a^{-1}.

CSA/RG and CRL/RG ratios of inhalation doses are shown in Table 6. As with the ingestion dose comparison, effective doses from CSA and RG are compared, doses to critical organs for the two models are compared (in bold) or the effective dose of CSA is compared with the dose to critical organ of RG, and the CSA dose based on updated DCFs (CRL) is compared with RG for both effective and organ doses. Since there is so little difference in the inhalation models, the differences in results are dominated by the DCFs. The CSA effective doses are usually higher than RG's, while doses to critical organs calculated with the updated DCFs are almost always lower than RG's, and none are significantly higher.

The CSA/RG ratios for ^{14}C inhalation doses for both adult and infant for effective and critical organ doses are alarmingly small, but since ratios calculated from the updated DCFs are still tiny (although about twice as large as the CSA/RG ratio), one might assume that RG's DCFs are the ones that should be reexamined.

External Dose Pathways

Each model calculates dose from external deposition by multiplying the deposition on the ground at steady state by a series of parameter values describing default conditions.

Table 6
CSA/RG and CRL/RG Ratios for Inhalation Doses for Adults and Infants

Nuclide	ADULT				Nuclide	INFANT			
	Total body		Critical organ*			Total body		Critical organ*	
	CSA/RG	CRL/RG	CSA/RG	CRL/RG		CSA/RG	CRL/RG	CSA/RG	CRL/RG
H-3	1.0	1.8	1.0	**1.8**	H-3	0.9	1.5	0.93	**1.5**
C-14	0.047	0.058	0.0089	**0.011**	C-14	0.015	0.018	0.0029	**0.0035**
Cr-51	31	12	0.22	**1.2**	Cr-51	22	12	0.15	**1.3**
Mn-54	9.9	7.9	0.044	**0.14**	Mn-54	3.2	6.6	0.016	**0.13**
Fe-59	11	11	0.11	**0.43**	Fe-59	8.2	7.1	0.077	**0.41**
Co-58	53	32	0.12	**0.54**	Co-58	27	22	0.063	**0.52**
Co-60	1.5E+2	65	0.37	**1.8**	Co-60	79	41	0.21	**1.6**
Zn-65	3.8	1.9	0.21	**0.8**	Zn-65	2.2	2.0	0.10	**0.70**
Sr-89	46	28	0.29	**1.8**	Sr-89	28	14	0.16	**1.5**
Sr-90	2.1	0.82	**0.17**	**0.91**	Sr-90	3.8	0.80	0.17	**1.2**
Zr-95	10	7.9	**1.7**	**0.71**	Zr-95	9.4	4.9	**2.2**	**0.71**
Nb-95	13	13	0.11	**0.51**	Nb-95	8.1	8.2	**0.76**	**0.49**
Mo-99	1.4E+3	1.3E+3	0.13	**0.69**	Mo-99	7.5E+2	7.5E+2	0.18	**1.5**
Ru-103	1.3E+2	1.4E+2	0.17	**1.0**	Ru-103	84	76	0.10	**0.93**
Ru-106	5.3E+2	2.4E+2	0.50	**3.3**	Ru-106	2.6E+2	1.1E+2	0.25	**2.9**
Te-132	4.0E+2	3.5E+2	3.0	**80**	Te-132	3.8E+2	2.8E+2	5.2	**8.9**
I-131	17	11	**1.0**	**0.70**	I-131	23	19	**1.0**	**0.77**
I-132	3.5	2.5	**0.92**	**0.44**	I-132	4.1	4.0	**0.89**	**0.49**
I-133	15	10	**1.0**	**0.63**	I-133	18	17	**0.91**	**0.66**
I-134	1.6	2.3	**0.69**	**0.27**	I-134	0.58	0.29	**0.80**	**0.31**
I-135	6.2	3.9	**1.0**	**0.53**	I-135	7.9	6.9	**1.0**	**0.58**
Cs-134	0.41	0.28	0.83	**0.51**	Cs-134	0.61	0.51	0.064	**0.081**
Cs-136	0.42	NA	0.83	NA	Cs-136	0.42	NA	0.17	NA
Cs-137	0.50	0.35	0.83	**0.47**	Cs-137	0.83	0.83	0.062	**0.093**
Ba-140	19	32	0.83	**0.11**	Ba-140	7.9	14	0.014	**0.094**
Ce-141	57	77	0.83	**1.5**	Ce-141	34	31	0.13	**1.1**
Ce-144	20	9.0	0.83	**3.2**	Ce-144	13	5.3	0.23	**2.6**

* Numbers in bold are the comparisons of critical organ to critical organ; all other comparisons called "critical organ" are CSA effective dose/RG dose to critical organ

Steady-state deposition (Bq m^{-2}) of CSA and RG is compared in Table 7. CSA deposition is about 16% that of RG (except for iodine) unless the radiological half-life of the nuclide is long (> 5 years), in which case the CSA/RG ratio is larger due to the "infinite" time of accumulation in CSA compared with the 15 year accumulation half-life in RG. The CSA/RG ratio for the iodines is about 0.31 because of higher deposition in CSA due to inclusion of particulate iodine. Deposition to ground for tritium and ^{14}C, although calculated, is not needed for any calculations in the ingestion pathway, since specific activity models are used, or for the external dose pathway, since neither nuclide contributes to effective or skin doses.

CSA/RG ratios for external doses are also compared in Table 7. The CSA/RG ratios for effective external doses are slightly less than the ratios for deposition (except for ^{132}Te and ^{140}Ba, which have very high CSA/RG ratios for DCF) even though the CSA has higher DCFs. The contribution to dose of low deposition in CSA is further reduced by the occupancy factor (0.2), dose reduction factor due to non-uniformity of surface (0.7) and shielding factor (i.e., fraction of outdoor dose received indoors) (0 for β and 0.4 for γ) relative to RG (1.0, none and 0.7 for both β and γ respectively), but these are mostly compensated by the CSA's higher DCFs. When the CRL/RG ratios for effective external dose are compared to CSA/RG ratios, there is little difference except for ^{95}Zr, ^{106}Ru and ^{144}Ce which are a factor of two or more higher for CRL/RG due to revised DCFs.

For skin dose from external deposition, the effect of the larger CSA/RG for DCFs for external skin dose are reflected in the CSA/RG ratio, for these ratios are higher, sometimes much higher than the ratios for effective dose, and some are greater than one. The large difference in ^{89}Sr is due to an extremely small DCF for skin in RG. In general, the CRL/RG ratios are consistently higher than CSA/RG ratios due to revised DCFs, and half are greater than one.

Immersion Pathways

In RG, the only immersion doses calculated are those from noble gases, whereas in CSA, immersion doses from all radionuclides are calculated. CSA has an occupancy factor (fraction of time an individual spends outside exposed to the plume) of 0.2, while the assumption in NUREG is an occupancy factor of 1. CSA uses a shielding factor of 0.9 for γ and 1.0 for β, while RG's shielding factor is 0.7 for the maximally exposed individual (compared here) and 0.5 for a member of the general population.

Table 7
CSA/RG and CRL/RG Ratios for Deposition and External Doses

	Deposition	External Dose: Effective		External Dose: Skin	
	CSA/RG	CSA/RG	CRL/RG	CSA/RG	CRL/RG
H-3	0.25				
C-14	1.5				
Cr-51	0.16	0.15	0.14	0.17	0.16
Mn-54	0.16	0.13	0.13	0.16	0.15
Fe-59	0.16	0.13	0.14	0.15	0.29
Co-58	0.16	0.13	0.14	0.16	0.20
Co-60	0.18	0.14	0.15	0.16	0.21
Zn-65	0.16	0.13	0.13	0.15	0.16
Sr-89	0.16	NC		4453	6607
Sr-90	0.41	NC		1.4	2.1
Zr-95	0.16	0.14	0.29	0.17	0.54
Nb-95	0.16	0.15	0.15	0.17	0.17
Mo-99	0.16	0.16	0.18	2.0	3.7
Ru-103	0.16	0.13	0.13	0.16	0.28
Ru-106	0.16	0.13	0.25	8.7	9.7
Te-132	0.16	1.5	1.5	4.4	6.5
I-131	0.31	0.27	0.28	0.40	2.0
I-132	0.31	0.25	0.26	0.80	1.2
I-133	0.31	0.31	0.35	2.2	3.8
I-134	0.31	0.30	0.32	1.1	1.5
I-135	0.31	0.22	0.24	0.74	1.2
Cs-134	0.16	0.12	0.13	0.17	0.33
Cs-136	0.16	0.14	NA	0.17	NA
Cs-137	0.43	0.37	0.37	1.1	2.6
Ba-140	0.16	1.2	1.2	5.2	7.8
Ce-141	0.16	0.15	0.18	0.24	3.4
Ce-144	0.16	0.15	0.68	38	46

In order to use the semi-infinite cloud model and appropriate dose conversion factors, it was assumed that the air concentration at 1000 m was uniform over the attenuation distance of each radionuclide. The conditions to use the semi-infinite cloud model in both NUREG (release height less than 80 m) and CSA (release height less than 50 m, distance from release 1 km or greater) were met.

The effective argon doses per concentration in air are very close, even though the parameter values and approaches are different (Table 8). CSA skin doses from immersion are just slightly higher than RG's, except for ^{88}Kr which is higher by a factor of three due to a skin dose conversion factor that is eighteen times higher than RG's. Using the slightly revised DCFs from CRL makes little difference between the CSA/RG and CRL/RG ratios (e.g., the CRL value of ^{88}Kr is still sixteen times higher than RG's).

Table 8
CSA/RG and CRL/RG Ratios for Immersion Dose

	Immersion Dose: Effective		Immersion Dose: Skin	
Nuclide	CSA/RG	CRL/RG	CSA/RG	CRL/RG
Ar-41	1.0	0.81	1.3	1.3
K-85m	0.95	1.0	1.1	1.1
Kr-87	1.0	1.1	1.2	1.2
Kr-88	1.4	1.4	3.1	2.8
Xe-133	0.81	0.89	0.99	1.1
Xe-135	0.94	1.0	1.1	1.2

SUMMARY AND CONCLUSIONS

The differences that exist between RG and CSA depend strongly on the assumptions made for an assessment. Structural differences are negligible. In this paper, when comparisons were made between the models as they could be run in an assessment, many of the options which make RG adaptable to different situations were not selected. Certainly, implementation of any of these options will result in doses even lower than those calculated here for comparison with CSA. Thus large differences may seem to exist between the two models, but they are mostly due to different assumptions employed in the assessment. Once the diets and delays to ingestion have been normalized between RG and CSA, the only other significant differences are due to the use of different parameter values. Most of the differences in parameter values are due to different dose conversion factors, and the use of the latest values in both models will correct these discrepancies. In addition, once the uncertainty in the calculations and parameter values is taken into account, a difference of a factor of two between CSA and RG will be shown to be unimportant since the 95% confidence interval on an ingestion dose might be expected to be at least a factor of five.

The five most important doses (Sv a^{-1}), whether effective or to a critical organ, calculated with realistic source terms are compared for CSA and RG in Table 9. Ingestion doses are dominated by ^{14}C for both RG and CSA because of the conservative assumptions of the scenario description: that all food is grown 1000 m from the stack. Changing a very few assumptions about diet will easily reduce ingestion doses. For example, if one assumes that 100% of the vegetables are grown 1000 m from the stack but that none of the animal produce is contaminated, the ^{14}C ingestion dose to an adult will be reduced to one-fourth in the CSA model. When revised DCFs, such as in CRL, are used in CSA and RG, RG's ^{14}C doses will drop more in line with CSA's. Also,

once the conceptual mistake for tritium in CSA is corrected (i.e., when more tritium is passed from forage to animals), the ingestion dose from tritium will rise and become quite comparable with RG's.

Tritium dominates inhalation dose predictions for both RG and CSA because of the amount released from CANDU reactors. Inhalation doses can be reduced by introducing a more realistic occupancy factor of less than one.

External doses may be higher than reported here by about a factor of three (the difference between the emission data estimated for these calculations and the average particulate emissions reported per CANDU unit). Nevertheless, they are low enough that they add little to overall dose.

Table 9
Top Five Ranked Doses (Sv per Annum) from RG and CSA Using Source Term Data from Table 1

Adult Ingestion				Infant Ingestion			
RG		CSA		RG		CSA	
C-14	2.1E-6	C-14	1.2E-6	C-14	9.7E-6	C-14	2.2E-6
H-3	1.8E-6	H-3	1.0E-6	H-3	2.7E-6	H-3	1.6E-6
Sr-90	8.4E-8	I-131	7.2E-8	I-131	3.1E-7	I-131	2.9E-7
Ru-106	1.8E-8	Sr-90	3.0E-8	Sr-90	8.1E-8	Nb-95	9.8E-9
Cs-137	8.1E-9	Cs-137	5.7E-9	Cs-137	3.3E-8	Sr-90	9.1E-9

Adult Inhalation				Infant Inhalation			
RG		CSA		RG		CSA	
H-3	1.3E-6	H-3	1.3E-6	H-3	6.6E-7	H-3	6.1E-7
C-14	3.7E-8	I-131	5.2E-10	C-14	5.5E-8	I-131	6.8E-10
Sr-90	1.0E-9	C-14	3.3E-10	I-131	6.7E-10	I-133	2.9E-10
I-131	5.4E-10	I-133	1.9E-10	Sr-90	4.2E-10	C-14	1.6E-10
I-133	2.0E-10	Sr-90	1.7E-10	I-133	3.2E-10	Sr-90	1.0E-10

External				Immersion			
RG		CSA		RG		CSA	
Cs-137	8.9E-9	Cs-137	9.9E-9	Kr-88	5.5E-7	Kr-88	1.7E-6
Sr-90	3.9E-9	Sr-90	5.4E-9	Xe-133	3.2E-7	Xe-135	3.3E-7
Cs-134	2.1E-9	Ce-144	5.9E-10	Xe-135	3.0E-7	Xe-133	3.1E-7
Co-60	1.6E-9	Ru-106	5.5E-10	Ar-41	2.1E-7	Ar-41	2.7E-7
Mn-54	3.0E-10	Cs-134	3.6E-10	Kr-87	2.0E-7	Kr-87	2.3E-7

Differences in doses from noble gases are slight, with the exception of ^{88}Kr with a skin dose three times higher in CSA than in RG. Immersion dose from all noble gases in general can be reduced by the use of more realistic parameter values for shielding and outdoor occupancy.

When intercomparing two models, there can be no "right" or "wrong" , "good" or "bad" answer. When models agree, it is hoped that the agreement is based on sound scientific evidence; if they disagree, the reasons for the disagreements should be found. This paper has drawn attention to important differences between CSA and RG which should be resolved. Some answers may be found in more up-to-date parameter values and in correcting some errors, but testing the models with independent data sets will be the only way to resolve which model produces predictions closest to what was measured in a real situation, using site-specific data in the models.

REFERENCES

(1) CANADIAN STANDARDS ASSOCIATION, "Guidelines for Calculating Derived Release Limits for Radioactive Material in Airborne and Liquid Effluents for Normal Operations of Nuclear Facilities", Canadian Standards Association, Rexdale, Ontario, 1987, CAN/CSA-N288.1-M87

(2) U. S. NUCLEAR REGULATORY COMMISSION, "Calculation of Annual Doses to Man from Routine Release of Reactor Effluents for the Purpose of Evaluating Compliance with 10 CFR Part 50, Appendix I", USNRC Office of Standards Development, Washington, D.C., 1977, Regulatory Guide 1.109.

(3) QINSHAN NUCLEAR POWER CORPORATION, "Qinshan Environmental Impact Report", 1996.

(4) NEIL, B.C.J., "Annual Summary and Assessment of Environmental Radiological Data for 1988", Ontario Hydro Health and Safety Division Report, 1988, SSD-AR-88-01.

(5) SUTHERLAND, J.K. , "Environmental Radiation Monitoring Data for Point Lepreau Generating Station, January 01, 1994 - December 31, 1994", New Brunswick Electrical Power Commission, Health Physics Department Report HP-07000-95-1.

(6) BOSS, C.R., "Talk entitled "Radioactive Emissions from Qinshan Phase 3 (2xCANDU6 [700MWe])", 1996.

(7) KOPEC, " Normal Operation Dose Analysis", Translated from the Korean, 1996.

(8) INTERNATIONAL ATOMIC ENERGY AGENCY, "International Basic Safety Standards for Protection against Ionizing Radiation and for the Safety of Radiation Sources", IAEA, Vienna, Safety Series No. 115-I (Interim Edition), 1994.

(9) AUDET, M.C. AND J.C. BAKER, "Derived Release Limits for Airborne and Liquid Effluents from Chalk River Laboratories during Normal Operations", Atomic Energy of Canada Limited, RC-1731 (Rev. 0), 1996.

(10) BIOSPHERIC MODEL VALIDATION STUDY, "Final report", Stockholm, Swedish Radiation Protection Institute, BIOMOVS Technical Report 15, 1993.

(11) BIOSPHERIC MODEL VALIDATION STUDY II, "An Overview of the BIOMOVS II Study and its Findings", Stockholm, Swedish Radiation Protection Institute, BIOMOVS II Technical Report 17, 1996.